Fabrication, Oxidation, and Combustion of Nanoscale Magnesium Diboride and Tetraboride

Andre Molina, Miguel J. Camarena, Evgeny Shafirovich*

Department of Aerospace and Mechanical Engineering, The University of Texas at El Paso, 500 W. University Ave., El Paso, TX 79968, USA

Abstract

The difficult ignition and low combustion efficiency of boron particles decrease the performance of boron-loaded, fuel-rich propellants for solid fuel ramjets and ducted rockets. One approach to solving this problem involves the use of magnesium diboride (MgB_2), which ignites easier than boron. Magnesium tetraboride (MgB_4) offers greater energy density owing to its higher boron content. However, the effect of B/Mg ratio on the ignition and combustion is unknown. Additionally, while nanoscale MgB_2 particles and quasi-2D structures are promising energetic additives, the oxidation and combustion properties of nanoscale MgB_4 have not been explored. To address these knowledge gaps, the present work included synthesis and high-energy ball milling of MgB_2 and MgB_4 powders, thermogravimetric analysis (TGA) of their oxidation, and combustion experiments with thin layers of the obtained powders. Comparison of two synthesis routes (a solid-state reaction in a tube furnace and combustion synthesis) has shown that the former is the superior method for producing magnesium borides. TGA has revealed that oxidation of both MgB_2 and MgB_4 results in a high conversion into the oxides (88-91%), far exceeding the low conversion of boron (62.5%). MgB_4 begins to oxidize rapidly at a much lower temperature (~900 °C) than MgB_2 (~1200 °C). The burning rates of milled MgB_2 and MgB_4 are about eight and five times, respectively, faster than that of submicron boron. Magnesium borides exhibit a stable, sustained boron flame, needed for high combustion efficiency, whereas physical Mg/B mixtures undergo Mg-driven "flash" combustion.

Keywords: Combustion of metals; Solid fuels; Propellants; Boron

*Corresponding author.

Novelty and significance statement

Magnesium diboride (MgB_2) is recognized as a promising energetic additive to fuel-rich propellants for solid fuel ramjets and ducted rockets. The present work is the first systematic investigation into the synthesis, oxidation, and combustion of its more energetic but less understood counterpart, magnesium tetraboride (MgB_4). The work has revealed a fundamental performance trade-off: MgB_4 offers a lower ignition temperature and greater energy density, while nanoscale MgB_2 provides superior burning rate. The gained insights into the combustion of magnesium borides will help fully utilize the great potential of boron as fuel for air-breathing propulsion.

1. Introduction

Boron-loaded, fuel-rich propellants for solid fuel ramjets and ducted rockets have the potential to dramatically increase the range of missiles and projectiles. However, the formation of a liquid boron oxide (B_2O_3) layer hinders ignition of boron particles and reduces combustion efficiency of boron-based fuels and propellants [1–5]. One approach to the improvement of boron combustion is based on the addition of magnesium (Mg), which ignites much easier than boron. The addition of magnesium has been achieved via several routes, including the mixing of magnesium and boron powders [6–8], the formation of composite particles [9–13], and the use of magnesium borides as a replacement for boron [9,13–16]. However, magnesium powder is susceptible to degradation over time [17–19]. Compared to Mg/B mixtures and composites, chemically bonded magnesium borides (MgB_x) offer thermal stability and slow aging [11]. Magnesium diboride (MgB_2) has been studied more than any other MgB_x phase for propulsion applications and because it was considered a promising superconductor. Recently, it has been tested as an additive to solid fuels for hybrid rockets. When added to paraffin-based fuels, MgB_2 burned completely, unlike boron, while also increasing the fuel's regression rate and density [20,21]. Because of the higher boron content, magnesium tetraboride (MgB_4) is potentially a more energetic additive than MgB_2. Figure 1 shows the calorific values of Mg, Al, B, MgB_2, and MgB_4, calculated using the standard enthalpies of formation

of MgO (-601.24 kJ/mol), Al_2O_3 (-1271.94 kJ/mol), B_2O_3 (-1675.69 kJ/mol), MgB_2 (-91.96 kJ/mol), and MgB_4 (-105.02 kJ/mol) [22]. The figure also shows the calorific values of Mg/2B and Mg/4B mixtures. It is seen that both MgB_2 and MgB_4 release more heat per unit mass than aluminum, the most common metal fuel ingredient of solid rocket propellants. It is also seen that MgB_4 is more energetic than MgB_2 and that the chemical bonds in MgB_2 and MgB_4 only slightly decrease the released heat.

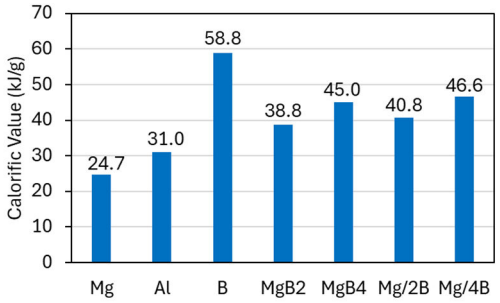

Fig. 1. Calorific values of Mg, Al, B, MgB_2, MgB_4, and Mg/B mixtures.

To improve the performance of solid fuels and propellants with these additives, it is necessary to understand the decomposition and oxidation of magnesium boride particles. This information is also important for safe handling and storing these powders and propellants. Guo et al. [23] studied decomposition and oxidation of MgB_2 powders at temperatures up to 1400 °C using thermogravimetric analysis (TGA), X-ray diffraction (XRD) analysis, and scanning electron microscopy (SEM). They have shown that the decomposition process of MgB_2 includes four stages with the consecutive formation of MgB_4, MgB_7, MgB_{20}, and B, where each stage also involves the release of Mg vapor. Rapid oxidation of MgB_2 in air starts at 600 °C. With increasing the temperature, four oxidation stages take place consecutively; they correspond to the four decomposition stages.

Liang et al. [15] studied combustion of Mg, B, and MgB_2 powders, ignited by a laser beam apparently in air (the gas environment was not reported), using high-speed video recording and emission spectroscopy. The ignition delay time of MgB_2 was 24 times shorter than for B and even shorter than for Mg, which confirms the high ignitibility of MgB_2. The ignition of each powder resulted in a vigorous combustion with sparks. The emission spectrum of MgB_2 during this stage showed lines of gaseous Mg, MgO, and BO_2. This stage was followed by stable combustion for each powder. The emission of MgB_2 was less intense during that stage, and it was difficult to identify the spectral lines of gaseous compounds. XRD analysis of the condensed products of MgB_2 combustion has shown peaks of MgB_2, MgB_4, MgB_7, MgB_{12}, MgO, B_2O_3, and $Mg_3B_2O_6$. This clearly indicates the presence of unreacted material and the occurrence of several decomposition and oxidation stages.

Guo et al. [24] obtained emission spectra of single MgB_2 and MgB_4 particles (median diameter: 4-5 μm) burning in $O_2/H_2O/CO_2/N_2$ gas mixture generated by combustion of $CH_4/O_2/N_2$ mixture in a flat-flame burner. The spectra of Mg and B particles were also obtained for comparison. Like in the work [15], the spectrum of MgB_2 contained the lines of Mg, MgO, and BO_2. The evolution of the spectrum showed that combustion of Mg dominated at the beginning but diminished with time. The spectra of MgB_4 were similar, but the combustion of Mg was less pronounced. The authors also prepared agglomerates of B, MgB_2, and MgB_4 particles in an HTPB matrix and studied their combustion in the same burner. The burning times of agglomerated MgB_2 and MgB_4 particles were shorter than those of agglomerated B particles. These results show that the combustion behavior of MgB_4 is similar to that of MgB_2 but do not allow for the conclusion to be made on which compound has better combustion characteristics. A recent study by Xu et al. compared the combustion properties of MgB_2 with other borides (AlB_2, TiB_2, SiB_6, B_4C), yet MgB_4 remains unexplored [25].

The combustion of magnesium borides may depend on the synthetic method used for their preparation. Usually, magnesium borides are synthesized from the elements, i.e., through the reactions between Mg and B powders at high temperatures. Synthesis in a furnace (in an inert gas or vacuum) allows for precise control over the temperature profile but requires external energy input and long processing times. In contrast, self-propagating high-temperature synthesis (SHS), which is one of combustion synthesis techniques [26,27], potentially offers a rapid and energy-efficient route for boride production. However, although the low enthalpies of formation of magnesium borides are a favorable factor for their use in propellants, they make SHS problematic. The adiabatic flame temperatures of stoichiometric mixtures for the formation of MgB_2 and MgB_4, calculated at constant pressure (1 atm) with THERMO (version 4.3) software [28], are equal to 1614 K and 1310 K, respectively. Although these relatively low temperatures do not exclude the possibility of self-sustained combustion wave propagation, it is difficult to achieve it in practice. Numerous researchers tried to fabricate MgB_2 by combustion synthesis. They usually added heat by placing the Mg/B mixture into a furnace [29–31]. In some experiments, it was possible to turn off the furnace and observe self-sustained combustion in the thermal explosion mode [32]. It was also possible to obtain MgB_2 via the so-called chemical oven technique, where the Mg/B mixture is surrounded by a highly exothermic Ti/C or Ti/B mixture, which provides heat for Mg/B combustion [33]. The lower adiabatic flame temperature of the mixture for MgB_4 synthesis implies that it may be even more difficult to fabricate it by SHS.

Post-synthesis treatment may also affect the properties of boride powders. Recently, MgB_2, mechanically activated by planetary ball milling, was compared with original (−100 mech size) MgB_2 powder and quasi-2D boron-based nanostructures (nanodots, nanograins, and nanosheets), obtained by sonication-assisted dissolution and recrystallization of MgB_2 crystals in water [14]. Owing to enhanced surface area and mesoporous structure, the mechanically activated MgB_2 powder has shown greater potential as a catalytic and energetic additive to ammonium perchlorate than pristine MgB_2 and quasi 2D nanostructures. However, the oxidation and combustion properties of nanoscale MgB_4 remain unknown.

The objective of the present work was to explore the oxidation and combustion of MgB_4 in comparison with MgB_2 and Mg/B mixtures. MgB_2 and MgB_4 were fabricated by combustion synthesis and by heating in a tube furnace, and ground to the nanoscale using high-energy ball milling. X-ray diffraction analysis and scanning electron microscopy were used to characterize the powders. The decomposition and oxidation of the obtained magnesium borides were investigated by thermogravimetric analysis. Their combustion was studied using laser ignition, high-speed video recording, and time-resolved optical spectroscopy. Comparative experiments with physical Mg/B mixtures were also conducted.

2. Experimental

Magnesium borides were synthesized using magnesium powder (99.8%, –325 mesh, Thermo Fisher Scientific) and amorphous boron powder (≥98% pure, <1 μm, STREM Chemicals). The boron and magnesium powders were mixed using a three-dimensional inversion kinematic mixer (Bioengineering Inversina 2L) at two B/Mg molar ratios, 2:1 and 4:1. To account for the volatility of magnesium during the heating process, B/Mg mixtures with a 10% and 20% excess of Mg were also prepared. The mixtures were compacted into cylindrical pellets (diameter: 13 mm) using a trapezoidal die and a uniaxial hydraulic press (force: 35–40 kN).

The B/Mg mixtures were converted into magnesium borides by combustion synthesis and by heating in a tube furnace. Initially, there were several attempts to achieve SHS in the Mg/B mixtures mechanically activated through high-energy ball milling at different parameters. However, all those attempts failed, and the combustion synthesis was performed using the chemical oven technique, where an Mg/B pellet was placed into a ceramic crucible and surrounded by 4-8 g of a Ti/B mixture (1:2 molar ratio) arranged in an annular layer. The synthesis was conducted in a laser ignition setup [34,35]. The crucible was positioned within a stainless-steel windowed chamber, which was then purged with ultrahigh-purity argon three times. The Ti/B mixture was ignited by an infrared beam of a CO_2 laser (Synrad Firestar ti-60), leading to the ignition and combustion of the Mg/B mixture. During this process, according to thermocouple measurements, the temperature within the crucible increased at a rate as high as 500 °C/s.

In the second method, the Mg/B pellet was placed into an alumina crucible, which was then closed with an alumina lid and placed inside the tube furnace (MTI GSL-1500x). The furnace was purged with argon three times, and argon was allowed to flow for 30 min at 0.3 L/min. Next, the furnace was heated under 0.8 L/min argon flow at a rate of 5 °C/min to a desired temperature. Since synthesis of MgB_2 and MgB_4 requires temperatures of 750 and 1050 °C, respectively [36,37], the 2:1 B/Mg samples were heated to 750 °C, and the 4:1 B/Mg samples were heated to 1050 °C, with both temperatures held for 2 h. Finally, the pellet was cooled to room temperature at a rate of 5 °C/min.

High-energy ball milling at parameters described in work [38] was employed for the mechanical activation of the mixtures before combustion synthesis and for producing nanoscale magnesium borides. 0.8 g of the powder was placed into zirconia-coated vials with 3 mm or 12.7 mm zirconia balls (ball-powder mass ratio: about 25). The milling was performed using a shaker mill (SPEX SamplePrep 8000D) inside an argon-filled glove bag. The process consisted of four to sixteen intervals, each comprising 1 hour of milling followed by 1 hour of cooling. After milling, the powder was left to cool to room temperature, and the milling balls and large agglomerates were separated from the powder using 1.7 mm and 150 μm sieves.

Thermogravimetric analysis (Netzsch STA 449 F3 Jupiter) was conducted to examine the high-temperature decomposition and oxidation of Mg, B, and magnesium borides. 1-2 mg of the tested powder was placed into an alumina crucible (85 μL) and heated from 25 °C to 1550 °C at a rate of 10 °C /min in a flow of argon (to study decomposition) or oxygen (to study oxidation). The flow rate was 50 mL/min in both cases.

The combustion characteristics of the synthesized powders were studied in the laser ignition setup mentioned above. All reported experiments were performed three times to ensure the results were reproducible. To determine the linear burning rate, powder was spread into a machined rectangular groove (40×10×1 mm) on a brass plate. The chamber was purged three times with ultrahigh-purity argon and subsequently filled with oxygen to a pressure of 90 kPa (near local atmospheric pressure). The sample was ignited near one end by the CO_2 laser (2.0±0.3 mm beam diameter) using a single 0.1 s pulse at a power of 32 W (measured with a Synrad powermeter). The propagation of the combustion front was recorded at 3000 fps by a high-speed camera (Phantom v1210) equipped with a macro lens (Nikon AF NIKKOR 60 mm f/2.8D), and the average propagation velocity

(linear burning rate) was determined based on the measured time. The condensed combustion products were collected from the rectangular groove for analysis. Phase compositions of synthesized borides and combustion products were determined by powder X-ray diffraction analysis (PANalytical Empyrean 2). The particles were also examined using scanning electron microscopy (SEM Hitachi s4800).

For spectral analysis of the flame, powder was packed into a cylindrical well (5 mm diameter×1 mm depth) machined into a brass plate. The sample was ignited under the atmospheric and laser conditions described above. The emitted light was analyzed by a spectrometer (AvaSpec-ULS2048CL-EVO-RS-UA).

3. Results and discussion

3.1 Synthesis and nanoscaling of magnesium borides

Figure 2 presents the XRD patterns of magnesium borides with B/Mg ratios of 2:1 and 4:1, synthesized using the tube furnace and the chemical oven technique. At the 2:1 ratio, the patterns of products obtained by both methods are virtually identical. In contrast, significant differences are observed at the 4:1 ratio. The tube furnace yielded MgB_4 and MgO, while the chemical oven also produced a high content of MgB_2. The latter was apparently due to significant evaporation of Mg during the combustion synthesis. Mechanically activation of the mixtures before combustion synthesis resulted in only minimal or negligible improvements. Due to the complexity of the chemical oven technique, waste material associated with the booster mixture, scalability issues, and its inability to produce high-quality MgB_4, it was decided that the tube furnace would be the primary method of synthesis in the present work.

Liquid-phase exfoliation of MgB2 has been successfully demonstrated [39,40], and its potential for solid propellant applications has also been explored [41]. While exfoliated layers may offer enhanced reactivity due to increased surface area, liquid-phase processing introduces significant variables, such as solvent compatibility, complex drying requirements, and a higher risk of surface oxidation. In contrast, dry (solvent-free) ball milling offers a scalable preparation route suitable for industrial production of ramjet fuels. Therefore, in the present work, we prioritized the robust, engineering-focused approach of dry milling, following the procedure [38] with minor modifications. SEM imaging (Fig. 3) has revealed that high-energy ball milling is effective regardless of the initial composition of the milled powder. The formed particles have an irregular shape. All of them are clearly less than 500 nm in size, with some being as small as 100 nm or less. Figure 4 shows the XRD patterns of the powders before and after milling. After four hours of milling, peak broadening is seen, which is evidence of reduced crystallite size. It should be noted that for MgB_4, the XRD pattern also shows a distorted crystal structure with altered relative intensities.

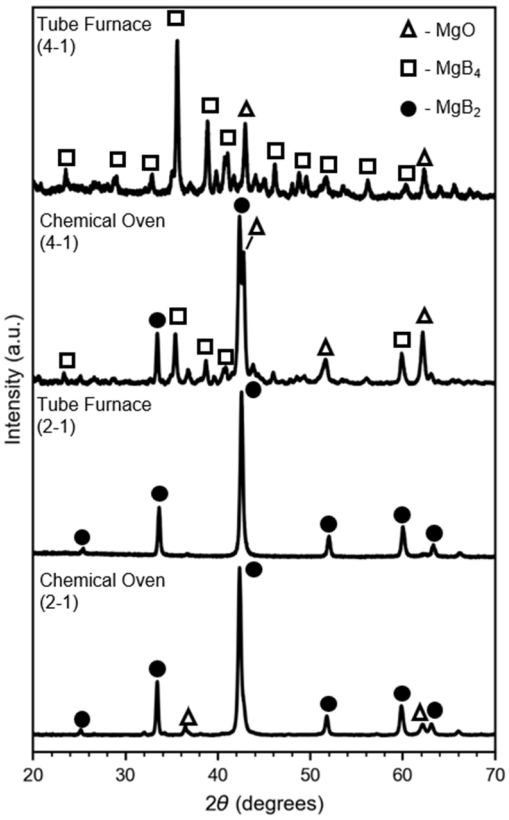

Fig. 2. XRD patterns of MgB_2 and MgB_4, synthesized using a tube furnace and the chemical oven.

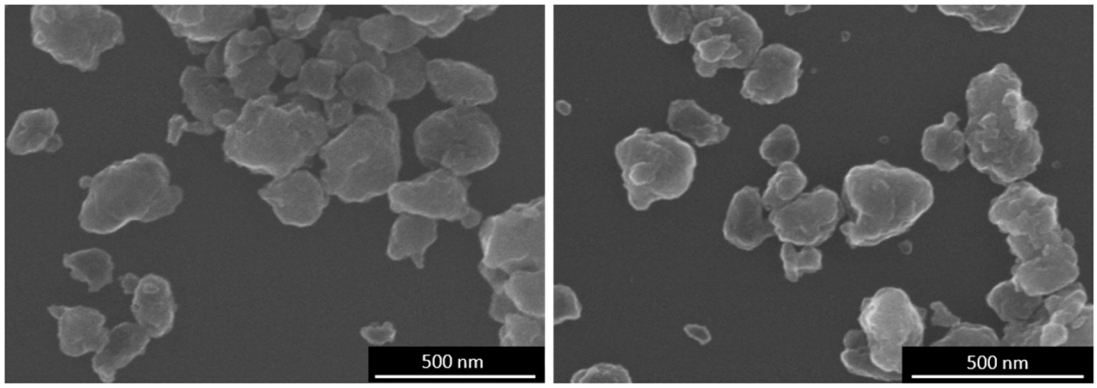

Fig. 3. SEM images of MgB_2 (left) and MgB_4 (right) particles after milling.

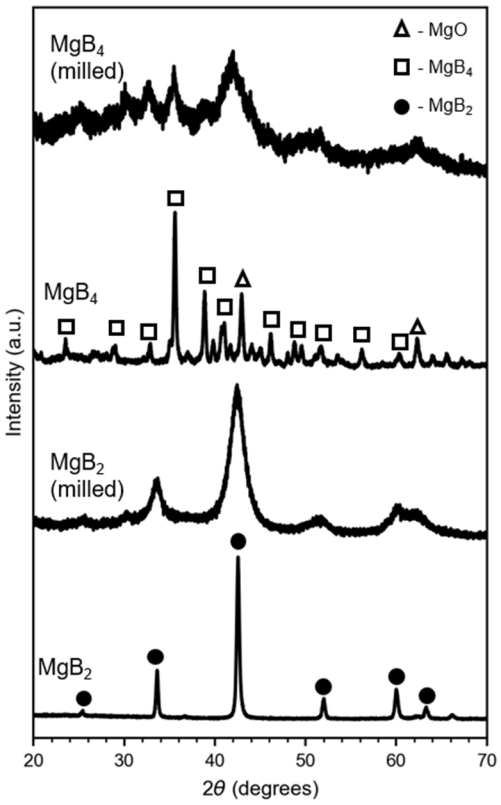

Fig. 4. Evolution of MgB_2 and MgB_4 XRD patterns during milling.

3.2 Decomposition and oxidation of magnesium borides

Figure 5 shows the thermogravimetric curves for decomposition of MgB_2 and MgB_4 in an argon flow. The curve for MgB_2 aligns closely with prior work [23], which showed a multi-step decomposition. At a temperature of about 900 °C, MgB_2 starts to decompose to form MgB_4 and Mg, which is vaporized due to its significant saturated vapor pressure. However, the formed MgB_4 layer slows down the diffusion of Mg and hence its evaporation. With approaching the Mg boiling point (around 1100 °C), MgB_4 decomposes to MgB_7 and Mg, which immediately evaporates. Again, the formed MgB_7 layer inhibits the diffusion and hence evaporation of Mg. Further increase in temperature apparently leads to the decomposition of MgB_7 to MgB_{20} and Mg vapor [23]. The TG curve for MgB_4 shows that its decomposition starts at around 1000 °C, which correlates with the decomposition of MgB_4 in the TG curve for MgB_2.

Figure 6 shows the thermogravimetric curves for oxidation of MgB_2 and MgB_4 in an O_2 flow, including samples ball-milled for 4 h. For comparison, the TG curves for Mg and B are also shown. The oxidation of Mg to MgO is complete (100% conversion) by 600 °C, which is explained by the non-protective properties of the MgO surface layer. The oxidation of boron, however, is much less efficient; it includes initial rapid oxidation at around 600 °C followed by a much slower increase in mass and then by its drop at around 1400 °C. To our knowledge, the observed linear oxidation law during the second stage of boron oxidation in TGA has not been explained in the literature. The reaction mechanisms during the first and second stages may include the formation of B-O solution, $(BO)_n$ polymer, boron suboxide (B_6O), and B_2O_3 [5,42,43] The final drop at around 1400 °C is caused by the evaporation of the formed boron oxides. The maximum extent of conversion (before the final drop) was only 62.5%.

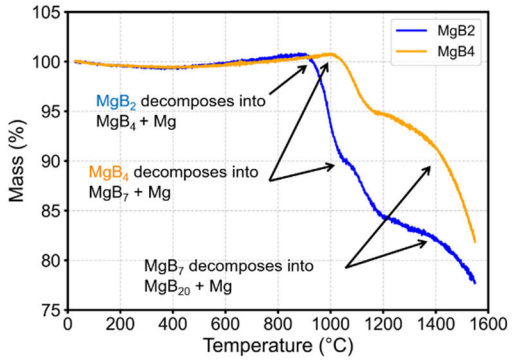

Fig. 5. TG curves for decomposition of MgB_2 and MgB_4.

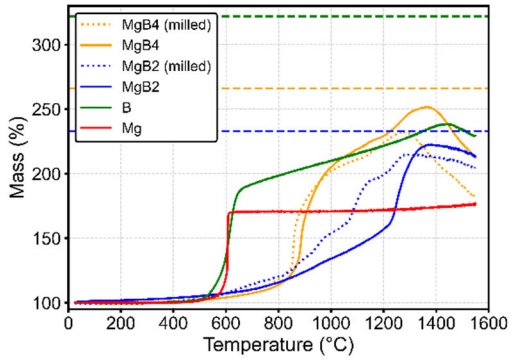

Fig. 6. TG curves for oxidation of Mg, B, MgB_2, and MgB_4. Dashed lines show the theoretical mass gains for B, MgB_2, and MgB_4.

The TG curves for the oxidation of the borides are different from those for Mg and B. In general, they show a relatively slow initial increase in mass followed by a much faster increase and then the final drop like for boron. The TG curve for oxidation of milled MgB_2 correlates with the MgB_2 decomposition curve like in prior work [23]. Each decomposition stage releases Mg vapor, which is immediately oxidized, contributing to the mass increase.

In contrast to MgB_2, the rapid mass increase of MgB_4 begins between 800 and 900 °C, i.e., before the decomposition onset. However, the decomposition of MgB_4 does occur during its oxidation, which explains the slowdown of the mass gain followed by a new acceleration at 1100 – 1200 °C. The low (compared to MgB_2) temperatures required for the rapid oxidation of MgB_4 may be related to the lower content of Mg.

The observed faster oxidation of MgB_4 at temperatures over 900 °C implies that under conditions of a combustion chamber, the MgB_4 particles may ignite easier than MgB_2. Of course, this hypothesis needs experimental verification, which is beyond the scope of the present work. For the milled MgB_2 and MgB_4 samples, the onset of the initial oxidation step is shifted to lower temperatures, indicating enhanced reactivity due to mechanical activation, likely by introducing defects into the surface layer and by increasing the surface area.

In stark contrast to boron, the magnesium borides achieved much higher conversion under the same conditions, reaching 88% for MgB_2 and 91% for MgB_4. This high degree of conversion also implies that the initial oxide impurities in the as-synthesized powders were relatively low. Based on the about 90% final conversion, it can be estimated that these impurities are likely to reduce the materials' theoretical energy density by about 10%. It should be noted that the MgO impurities can be removed by acid leaching [36,44]. Milling slightly decreased the final conversion for the borides (83% for milled MgB_2 and 80% for milled MgB_4). A similar effect of milling has been seen in nano-Al particles [45], and the decreased conversion could be caused by the oxygen impurities in the glove bag during milling and oxygen exposure during handling. Comparison with the low conversion of boron clearly shows that the borides not only oxidize much faster than boron at elevated temperatures but also achieve a more complete oxidation.

3.3. Combustion behavior and burning rate

To illustrate how the linear burning rate was determined, Figure 7 shows a schematic diagram and images of the combustion propagation over a layer of MgB_4 powder. Typical videos of combustion of Mg, B, and the two borides (each non-milled and milled) are presented in the Supplementary Material. The average propagation velocities of the combustion front were calculated based on distance and time, and the obtained values are presented in Fig. 8. A significant variation in combustion propagation velocity was observed across the samples. The amorphous boron powder, with a reported particle size within the range described as most reactive [46], burned at 91 mm/s. In comparison, the non-milled MgB_2 and MgB_4 powders burned at 188 mm/s and 180 mm/s, respectively. This doubling of the burning rate, despite the coarse particles of the borides compared to the submicron boron, underscores the superior intrinsic reactivity of the boride compounds, even in the presence of oxide impurities. This enhanced reactivity aligns with the high extents of conversion observed for the oxidation of the borides in the TGA experiments.

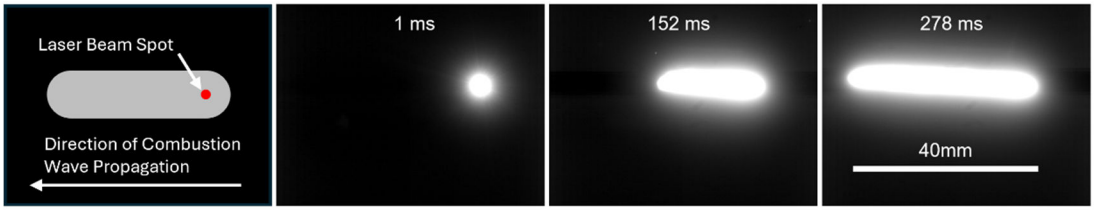

Fig. 7. Schematic diagram (left) and images of ignition and combustion propagation over MgB_4 powder layer. The camera was installed at an angle of 25° to the sample surface. Time zero is the onset of light emission.

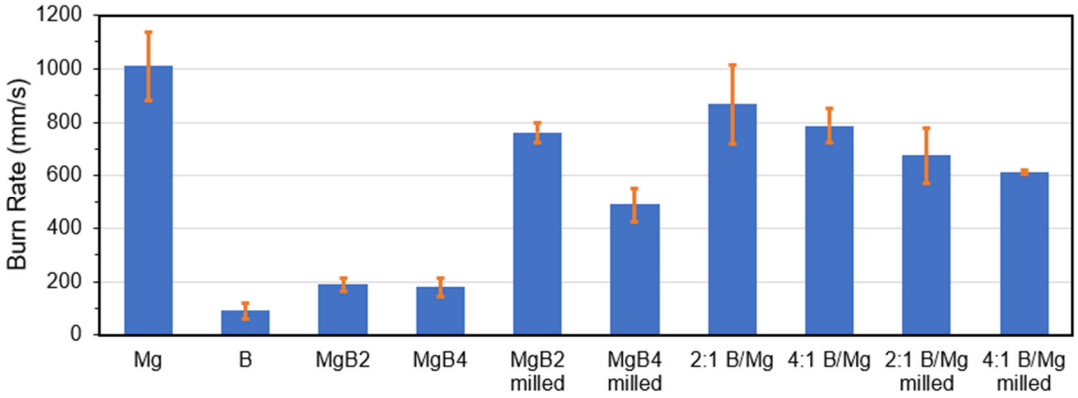

Fig. 8. Linear burning rates of Mg, B, MgB_2 (non-milled and milled), and MgB_4 (non-milled and milled) powders.

Milling of the boride powders significantly accelerated their combustion propagation. The burning rate of milled MgB_2 increased to 762 mm/s (a four-fold increase), while milled MgB_4 reached 489 mm/s (a 2.7-fold increase). When compared to pure boron, the milled MgB_2 and MgB_4 powders burned approximately 8.4 and 5.4 times faster, respectively. This highlights the profound effect of increased surface area and mechanically induced defects on combustion performance.

It is important to reconcile this dramatic increase in burning rate with the TGA results, which showed a slight decrease in the final conversion for milled powders. This apparent discrepancy highlights the different phenomena governing relatively slow oxidation in TGA versus rapid, self-propagating combustion. The lower final conversion of the milled particles in TGA is likely due to the passivating effect of an oxide layer formed during milling, whereas the reaction rate during rapid combustion increases with decreasing the particle size. The nanoscale particles produced by milling, as seen in the SEM images (Fig. 3), provide a significantly greater surface area for reaction. This leads to a drastically accelerated reaction rate and heat feedback, which dictates the propagation speed, even if the overall reaction completeness far behind the front is slightly lower.

For comparison, physical mixtures of boron and magnesium were also tested. The 2:1 B/Mg and 4:1 B/Mg mixtures showed high burning rates of 867 mm/s and 786 mm/s, respectively, approaching the combustion velocity of magnesium. Surprisingly, milling decreased the burning rates of the B/Mg mixtures (this is discussed in Section 3.5).

It should be noted that the burning rate determined based on luminosity propagation can be high but at incomplete conversion. For this reason, it is important to analyze the combustion products.

3.4. XRD analysis of combustion products

Figure 9 shows the XRD patterns of the products collected after combustion of Mg, B, MgB_2, MgB_4, 2:1 B/Mg mix, and 4:1 B/Mg mix powders. The XRD patterns for the precursor materials (Mg and B) reveal a significant difference in combustion efficiency. The pattern for combusted Mg shows conversion into crystalline magnesium oxide (MgO), although incomplete, apparently because of significant heat losses. Conversely, the pattern for combusted B is characterized by a large amorphous background and lack of distinct crystalline peaks, indicating a failure to fully convert into a stable oxide. The observed lack of crystalline B_2O_3 may be explained by its evaporation during combustion or its amorphization which would not be detected by XRD.

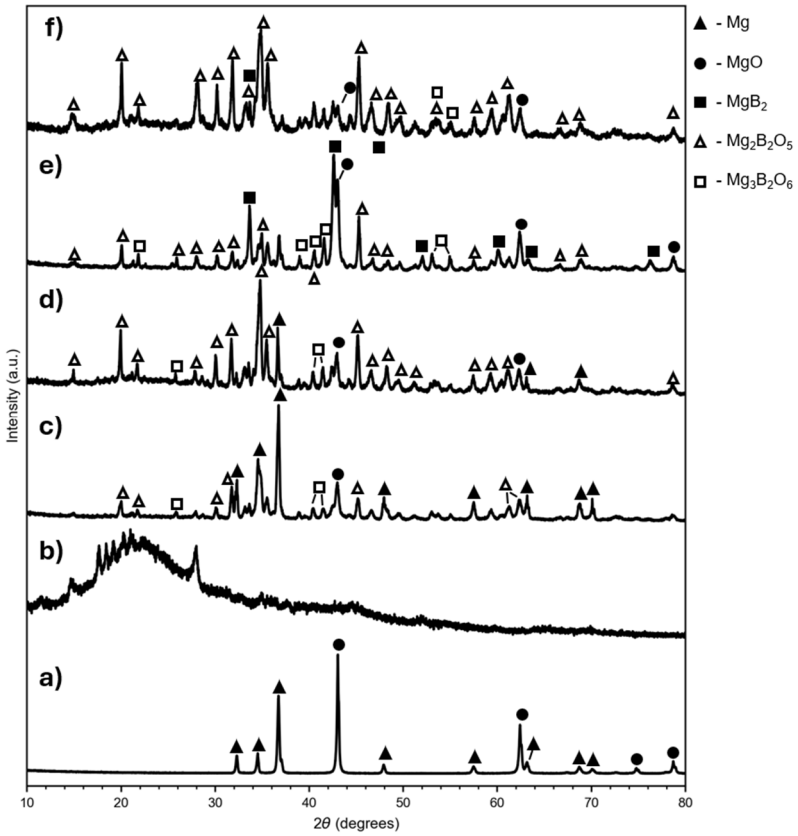

Fig. 9. XRD patterns of combusted (a) Mg, (b) B, (c) MgB_2, (d) MgB_4, (e) 2:1 B/Mg mix, and (f) 4:1 B/Mg mix powders.

The products of MgB_2 combustion contain a significant amount of free Mg. Other identified phases include MgO, magnesium pyroborate ($Mg_2B_2O_5$), and traces of magnesium orthoborate ($Mg_3B_2O_6$). It is worth mentioning that the formation of $Mg_2B_2O_5$ and $Mg_3B_2O_6$ was recently predicted in the DFTB-MD simulations of the reaction between Mg vapor and B_2O_3 surface [47]. The products of MgB_4 combustion contain more $Mg_2B_2O_5$ and less Mg, with traces of $Mg_3B_2O_6$ being still present. The combustion products of B/Mg mixtures also contain $Mg_2B_2O_5$ and $Mg_3B_2O_6$ but no unreacted Mg. Interestingly, along with MgO, MgB_2 was formed during combustion of Mg/2B mixture, and it remained unoxidized.

Magnesium pyroborate and orthoborate can be considered as the sums of MgO and B_2O_3 according to the equations:

$$Mg_2B_2O_5 \rightarrow 2MgO + B_2O_3 \quad (1)$$

$$Mg_3B_2O_6 \rightarrow 3MgO + B_2O_3 \quad (2)$$

On the other hand, the full oxidation of MgB_2 and MgB_4 (or Mg/2B and Mg/4B mixtures) should produce higher B_2O_3/MgO ratios:

$$MgB_2 + 2O_2 \rightarrow MgO + B_2O_3 \quad (3)$$

$$MgB_4 + 3.5O_2 \rightarrow MgO + 2B_2O_3 \quad (4)$$

The observed lack of B_2O_3 is explained by its evaporation during combustion (see Section 3.2). It should be noted that although the formation enthalpies of anhydrous $Mg_2B_2O_5$ and $Mg_3B_2O_6$ are unknown, the effect of their formation instead of MgO and B_2O_3 on the calorific value is likely small.

Figure 10 shows XRD patterns of the products collected after combustion of milled MgB_2, MgB_4, 2:1 B/Mg mix, and 4:1 B/Mg mix powders. No free Mg was detected in the combustion products of the milled MgB_2 and MgB_4. The products of milled MgB_4 and Mg/4B mix contain significant peaks of MgB_7, which is discussed in the next section.

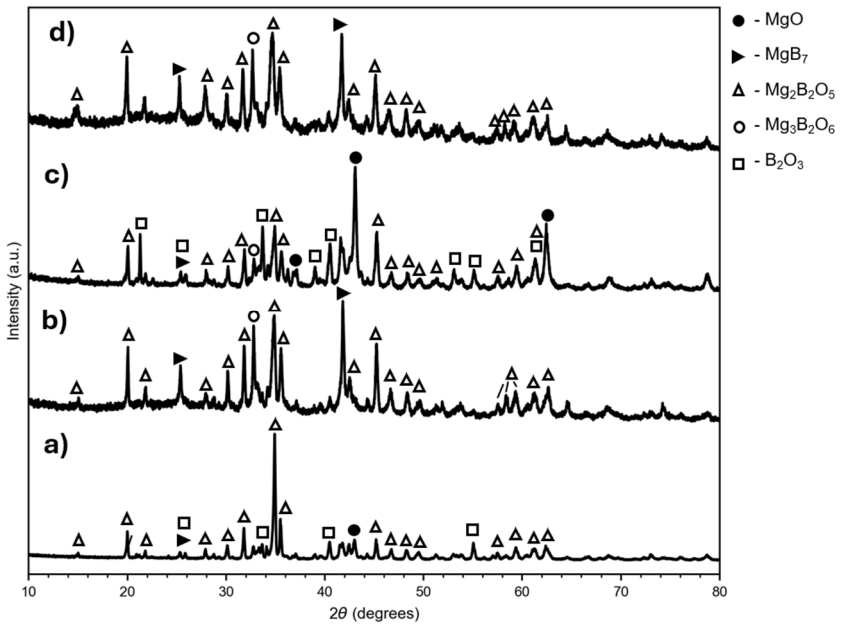

Fig. 10. XRD patterns of combusted milled (a) MgB_2, (b) MgB_4, (c) 2:1 B/Mg mix, and (d) 4:1 B/Mg mix powders.

3.5. Emission spectroscopy

Figure 11 presents the emission spectra at three key stages of combustion: peak intensity at the beginning, the midpoint of its burn time (midway), and the end point. The burn time itself, from ignition to burnout, was determined by applying an intensity threshold of 100 counts to the respective emission signal, a value selected for being well above the baseline noise. The spectrum of burning magnesium shows strong lines of Mg and MgO in ultraviolet range (350-400 nm) as well as at 498 and 518 nm. The sharp lines at 589, 671, and 766 nm belong to impurities of Na, Li, and K, respectively. The spectrum of burning boron shows the prominent BO_2 band system as in prior work [48,49]. The spectra of unmilled Mg/B mixtures appear to be superimposition of the Mg spectrum on the B one (the addition of UV lines and the overlap of the BO_2 line at 492 nm and MgO line at 498 nm). The spectra of unmilled borides are more similar to the one of boron but with the addition of UV emission. The spectra of milled mixtures and borides are qualitatively similar to those of unmilled ones.

To obtain more information from the spectra, following established methods, boron oxidation was tracked by monitoring the emission intensity at a wavelength of 547 nm (the peak of the BO_2 band system), while magnesium-containing species were tracked by using the excited neutral magnesium (Mg I) atomic line at 383 nm [50–52]. These wavelengths were chosen because a comparison with the individual combustion spectra of B and Mg confirmed they are free from mutual interference.

Figure 12 shows the full temporal profiles of BO_2 and Mg I emitted during combustion of the non-milled and milled powders. From these profiles, two primary metrics were calculated for comparison. The integrated B/Mg emission ratio ([BO_2] / [Mg I]) was used as a qualitative indicator of the relative contribution of boron versus magnesium oxidation. The average BO_2 emission rate (intensity/time) was calculated to quantify the overall intensity of the sustained boron flame. Table 1 shows these metrics along with the measured burning rates. The B/Mg ratio for MgB_4 was nearly an order of magnitude higher than for MgB_2, confirming a more dominant boron combustion phase for MgB_4, consistent with its higher boron content.

A particularly insightful finding emerges when comparing the linear burning rate with the average BO_2 emission rate. The sample with the highest burning rate, 2:1 B/Mg mix (867 ± 148 mm/s), does not produce the most intense sustained boron flame. In fact, its average BO_2 emission rate (275 ± 74 unit/s) is significantly lower than that of the much slower combustion of non-milled MgB_4 (180 ± 33 mm/s, 684 ± 182 unit/s). This inverse relationship suggests that "propagation velocity" and "boron flame intensity" are decoupled. The rapid combustion may be dominated by a transient, Mg-driven reaction front, whereas the slower and steadier combustion of non-milled MgB_4 allows for a more prolonged and complete boron oxidation phase, leading to a higher time-averaged emission intensity.

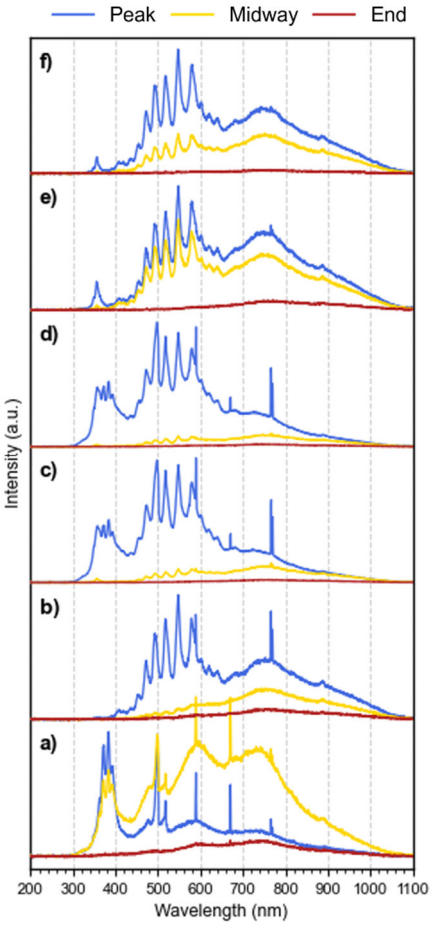

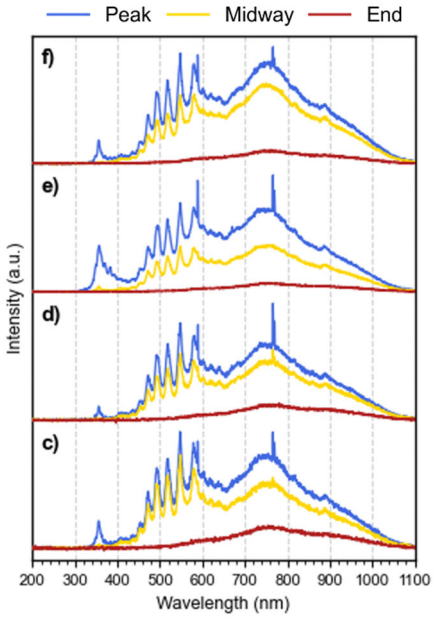

Fig. 11. Spectrograms of (a) Mg, (b) B, (c) 2:1 B/Mg mix, (d) 4:1 B/Mg mix, (e) MgB_2, and (f) MgB_4 powders, non-milled (left) and milled (right). Time zero is the onset of light emission.

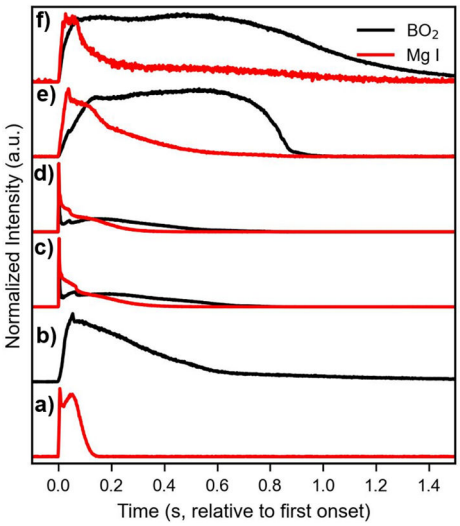

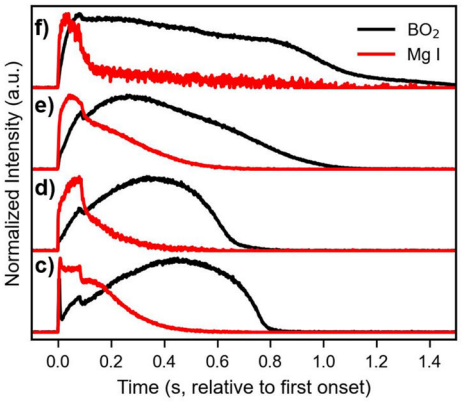

Fig. 12. Emission intensity as a function of time for (a) Mg, (b) B, (c) 2:1 B/Mg mix, (d) 4:1 B/Mg mix, (e) MgB_2, and (f) MgB_4 powders, non-milled (left) and milled (right). Time zero is the onset of light emission.

Table 1
Burning rates and spectroscopic metrics of magnesium borides and B/Mg mixtures.

Sample	Linear burning rate	Relative burning rate (vs. B)	B/Mg emission ratio	Average BO_2 emission rate	BO_2 emission time
	mm/s	-	-	a.u./s	s
Mg	1010 ± 128	11.1	-	-	-
B	91 ± 30	1	-	425 ± 172	1.98 ± 0.52
MgB_2	189 ± 24	2.1	4.9 ± 0.2	483 ± 136	0.99 ± 0.04
MgB_4	180 ± 33	2	34.6 ± 8.9-	684 ± 182	1.94 ± 0.21
MgB_2 (milled)	762 ± 38	8.3	3.7 ± 0.1	374 ± 102	1.06 ± 0.05
MgB_4 (milled)	489 ± 63	5.4	-*	341 ± 170	1.26 ± 0.17
2:1 B/Mg mix	867 ± 148	9.5	2.6 ± 0.8	275 ± 74	0.87 ± 0.16
4:1 B/Mg mix	786 ± 64	8.6	4.8 ± 1.9	332 ± 168	1.02 ± 0.28
2:1 B/Mg mix (milled)	677 ± 103	7.4	3.2 ± 0.1	257 ± 53	0.81 ± 0.02
4:1 B/Mg mix (milled)	613 ± 6	6.7	11.2 ± 1.4	276 ± 95	0.94 ± 0.17

* Unreliable due to a weak Mg I signal

The effect of milling on the boride compounds further clarifies this mechanistic distinction. For MgB_2, milling quadruples the burning rate but decreases the B/Mg emission ratio from 4.9 to 3.7. This trend suggests that nanoscaling primarily accelerates the initial, Mg-driven stage without proportionally enhancing the subsequent boron oxidation. In contrast, while milling more than doubles the burning rate of MgB_4, the B/Mg emission ratio for the milled sample becomes unreliable due to an especially weak Mg signal (Fig. 13). The consistently weak Mg emission from MgB_4, especially when compared to the robust signal from MgB_2, correlates with the observations of Guo et al. [24]. They noted that the emission spectrum of MgB_4 was closer to that of amorphous boron, with a diminished Mg signal compared to MgB_2.

The weak initial Mg signal we observed and the observations of reaction between molten Mg and B_2O_3 even at relatively low temperatures (500–650 °C) [7] provide clear support for the condensed-phase mechanism of MgB_4 combustion. This is also supported by the results of TGA studies. Indeed, the decomposition of MgB_4 to MgB_7 and Mg vapor begins at about 1000 °C (Fig. 5), but significant oxidation of MgB_4 takes place at much lower temperatures (Fig. 6), where Mg vapor cannot be involved. Further, the presence of MgB_7 phase in the products, reported in Section 3.4, indicates that the condensed-phase reaction between magnesium and boron oxide locally enriches the material with elemental boron, driving the formation of the boron-rich phase MgB_7. We therefore state that magnesium's primary role in MgB_4 combustion is the condensed-phase, thermite reaction with the initial and formed boron oxide. Interestingly, the decreased role of Mg vapor in the combustion mechanism of MgB_4 is similar to the decreased role of gas-phase oxygen in the combustion of nanothermites [53].

This mechanistic divergence between MgB_2 and MgB_4 may stem from the fundamental difference in the crystal structures of these compounds. The layered, graphene-like arrangement of MgB_2 may facilitate the release of Mg vapor, while the three-dimensional B_6 framework of MgB_4, with Mg atoms occupying voids, favors the condensed-phase reaction pathway [54,55]. In addition, the reduced crystallinity of milled MgB_4, observed in the XRD patterns (Fig. 4), could facilitate inward oxygen diffusion and hence promote the condensed-phase reaction.

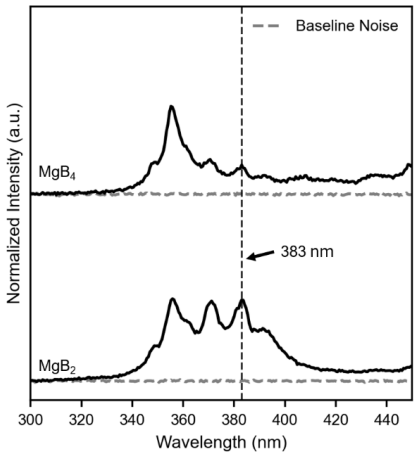

Fig. 13. Comparison of Mg I peaks (383 nm) in the emission spectra of MgB_2 and MgB_4

A direct comparison between the boride compounds and their corresponding elemental mixtures reveals the critical role of chemical bonding in achieving efficient boron combustion. While the physical mixtures exhibit high linear burning rates (Table 1), analysis of their time-resolved emission profiles (Fig. 12) shows a distinct mechanism. Both the 2:1 and 4:1 B/Mg mixtures are characterized by a violent, sharp emission peak at the onset of combustion, which then rapidly diminishes. This behavior suggests that the combustion front is driven by the vigorous ignition of magnesium particles, which provides a rapid initial propagation but fails to create conditions for a long-lived boron flame.

This flash combustion explains why the time-averaged BO_2 emission for both borides is nearly

double that of their mixture counterparts (Table 1). The combustion of physically mixed Mg and B may lead to the formation of metastable Mg-B intermediates. In contrast, the chemically bonded atomic arrangement in the pre-synthesized MgB_x potentially bypasses kinetic traps associated with these intermediates, facilitating a more direct pathway to stable products. As a result, the chemically bonded borides release their fuel components in a more controlled manner, leading to a more stable and sustained boron flame, even if their initial peak intensity is lower.

This conclusion is further supported by the B/Mg emission ratios. While the ratio for MgB_2 (4.9 ± 0.2) is moderately higher than for the 2:1 B/Mg mix (2.6 ± 0.8), the difference is dramatic for the more boron-rich compounds. The B/Mg emission ratio for MgB_4 (34.6 ± 8.9) is more than seven times greater than for the 4:1 B/Mg mix (4.8 ± 1.9). This indicates that the intimate, atomic-level bonding in MgB_4 is exceptionally effective at converting its high boron content into a strong, boron-specific flame signature. In the physical mixture, much of the extra boron likely fails to combust efficiently in the gas phase. Therefore, while physical mixing provides a potent ignition source, the chemical bonding within magnesium borides is superior for achieving sustained and efficient boron energy release.

Whereas the boride compounds represent a fuel arrangement on the atomic level, milling the physical mixtures is a mechanical attempt to create an intimate arrangement on the particle level. The effect of milling on the mixtures further underscores the importance of both stoichiometry and morphology, as evidenced by their distinct temporal emission profiles (Fig. 12). Milling the 2:1 B/Mg mix, i.e., a mixture with high mass fraction of ductile magnesium, apparently leads to the formation of large composite agglomerates. The resulting emission profile for Mg I exhibits significant instability: an initial peak is followed by a series of step-like drops and plateaus. This pulsating signal likely represents a multi-stage process where different concentrations of Mg particles are ignited and consumed sequentially, preventing the formation of a stable flame front and leading to decreased burning rates compared to the non-milled powder (see Fig. 8 and Table 1).

The boron-rich 4:1 B/Mg mix behaves differently. For this mixture, milling profoundly alters the combustion behavior. The initial, sharp Mg-driven emission peak seen in the non-milled sample is eliminated. The resulting temporal profile becomes steadier and closer to the profile of the MgB_4 compound. Apparently, a more uniform distribution of ductile magnesium among the boron particles after milling shifts the combustion from an explosive, Mg-initiated event to a more controlled, compound-like surface reaction and a relatively low burning rate. However, while the combustion dynamics become like that of MgB_4, the boron combustion efficiency does not. The BO_2 emission rate remains significantly lower (276 ± 95 unit/s vs. 684 ± 182 for MgB_4), highlighting the importance of the chemical bond for effective boron energy release.

4. Conclusions

The fabrication, oxidation, and combustion of MgB_2 and MgB_4 have been studied experimentally. Comparison of two synthesis routes (a solid-state reaction in a tube furnace and combustion synthesis) has shown that the former is the superior method for producing magnesium borides.

Thermogravimetric analysis has revealed that the oxidation of MgB_2 and MgB_4 results in a high conversion into oxides (88-91%), far exceeding the low conversion of boron (62.5%). MgB_4 begins to oxidize rapidly at a much lower temperature (~900 °C) than MgB_2 (~1200 °C), indicating a lower kinetic barrier to ignition under engine conditions.

Combustion experiments with thin layers of powders have shown that the synthesized magnesium borides burn much faster than submicron boron. High-energy ball milling further accelerates their combustion. The burning rates of milled MgB_2 and MgB_4 are about eight and five times, respectively, faster than that of submicron boron.

Emission spectroscopy revealed a fundamental difference in combustion mechanisms of magnesium borides and physical B/Mg mixtures. The atomic-level arrangement in MgB_2 and MgB_4 promotes a stable, sustained boron flame, needed for high combustion efficiency. In contrast, the physical mixtures undergo an Mg-driven "flash" propagation of combustion, which is less effective at utilizing the energy content of boron.

In summary, the present work provides a quantitative comparison of MgB_2 and MgB_4 combustion and demonstrates that nanoscaling is an effective strategy for enhancing their performance. While MgB_4 offers higher energy density and a lower oxidation onset temperature, milled MgB_2 burns faster than milled MgB_4. These insights into the combustion of magnesium borides will be useful in the development of fuel-rich, boron-loaded propellants for solid fuel ramjets and ducted rockets.

CrediT authorship contribution statement

Andre Molina: Investigation, Methodology, Writing – original draft. **Miguel Camarena:** Investigation. **Evgeny Shafirovich:** Conceptualization, Funding acquisition, Project administration, Writing – review & editing.

Declaration of competing interest

The authors declare that they have no known competing financial interests or personal relationships that could have appeared to influence the work reported in this paper.

Acknowledgment

This material is based upon work supported by the U.S. Department of Energy's Office of Energy Efficiency and Renewable Energy (EERE) under the award number DE-EE0010429.

Declaration of generative AI and AI-assisted technologies in the writing process

During the preparation of this work the authors used Gemini to improve the readability of the manuscript. After using this tool/service, the authors reviewed and edited the content as needed, and they take full responsibility for the content of the published article.

References

[1]. A. Gany, D.W. Netzer, Combustion studies of metallized fuels for solid-fuel ramjets, J. Propuls. Power 2 (1986) 423-427.

[2]. A. Gany, Y. M. Timnat, Advantages and drawbacks of boron-fueled propulsion, Acta Astronaut. 29 (1993) 181-187.

[3]. K.K. Kuo, R. Pein, Combustion of boron based solid propellants & solid fuel, CRC Press, Boca Raton, 1993.

[4]. W. Pang, L.T. De Luca, X. Fan, O.G. Glotov, F. Zhao, Boron-based fuel-rich propellant: properties, combustion, and technology aspects, Taylor & Francis, Boca Raton, 2019.

[5]. C.L. Yeh, K.K. Kuo, Ignition and combustion of boron particles, Prog. Energy Combust. Sci. 22 (1996) 511-541.

[6]. S.A. Hashim, S. Karmakar, A. Roy, Effects of Ti and Mg particles on combustion characteristics of boron-HTPB-based solid fuels for hybrid gas generator in ducted rocket applications, Acta Astronaut. 160 (2019) 125-137.

[7]. P. Ghildiyal, F. Xu, A. Rojas, Y. Wang, M. Chowdhury, P. Biswas, S. Herrera, R. Abbaschian, M.R. Zachariah, Magnesium-enhanced reactivity of boron particles: role of Mg/B_2O_3 exothermic surface reactions, Energy Fuels 37 (2023) 3272-3279.

[8]. E.T. Sandall, J. Kalman, J.N. Quigley, S. Munro, T.D. Hedman, A study of solid ramjet fuel containing boron-magnesium mixtures, Propuls. Power Res. 6 (2017) 243-252.

[9]. Y. Sun, H. Ren, Q. Jiao, M. Schoenitz, E.L. Dreizin, Oxidation, ignition and combustion behaviors of differently prepared boron-magnesium composites, Combust. Flame 221 (2020) 11-19.

[10]. X. Liu, K.-L. Chintersingh, M. Schoenitz, E.L. Dreizin, Reactive composite boron-magnesium powders prepared by mechanical milling, J. Propuls. Power 34 (2018) 787-794.

[11]. P.P.K. Agarwal, D. Jensen, C.-H. Chen, R. Rioux, T. Matsoukas, Synthesis and characterization of magnesium/boron solid solutions for energetic applications, ACS Appl. Energy Mater. 5 (2022) 6716-6723.

[12]. Y. Wang, Y. Yu, Preparation and characterization of boron-magnesium-titanium ternary composite powders, Coatings 15 (2025) 739.

[13]. C. Leuchtmann, D.F. Gallegos, G. Young, M. Schoenitz, E.L. Dreizin, Combustion of solid fuels containing boron, borides, and boron based composites in a solid fuel ramjet, Fuel 371 (2024) 132101.

[14]. H. Gunda, C. Ghoroi, K. Jasuja, Layered magnesium diboride and its derivatives as potential catalytic and energetic additives for tuning the exothermicity of ammonium perchlorate, Thermochim. Acta 690 (2020) 178674.

[15]. D. Liang, R. Xiao, H. Li, J. Liu, Heterogeneous decomposition and oxidation during combustion of magnesium diboride particles, Acta Astronaut. 153 (2018) 159-165.

[16]. F.K. Bulanin, A.E. Sidorov, S.A. Kiro, N.I. Poletaev, V.G. Shevchuk, Ignition of metal boride particle-air mixtures, Combust. Explos. Shock Waves 56 (2020) 57-62.

[17]. H. Nie, M. Schoenitz, E.L. Dreizin, Oxidation of magnesium: implication for aging and ignition, J. Phys. Chem. C 120 (2016) 974-983.

[18]. J. Oh, S. Jang, J.J. Yoh, On the pyrolysis mechanism of Magnesium-Teflon-Viton (MTV) igniters subjected to seasonal aging, Fuel 389 (2025) 134604.

[19]. J. Oh, Y. Lee, J.J. Yoh, On the oxidation kinetics of aging magnesium particles, Combust. Flame 249 (2023) 112597.

[20]. A.E.M. Bertoldi, M. Bouziane, D. Lee, P. Hendrick, C. Vandevelde, M. Lefebvre, C.A.G. Veras, Development and test of magnesium-based additive for hybrid rockets fuels, 2018 SpaceOps Conference, AIAA 2018-2383.

[21]. A.E. de Morais Bertoldi, R. Gelain, P. Hendrick, Characterization of magnesium diboride as an additive for paraffin-based fuel hybrid rockets, 9th European Conference for Aeronautics and Space Sciences, EUCASS 2022-6109.

[22]. M.W. Chase, NIST-JANAF Thermochemical Tables, Fourth Edition, J. Phys. Chem. Ref. Data Monograph 9 (1998) 1-1951.

[23]. Y. Guo, W. Zhang, D. Yang, R. Yao, Decomposition and oxidation of magnesium diboride, J. Am. Ceram. Soc. 95 (2012) 754-759.

[24]. Y. Guo, X. Zhou, W. Zhang, L. Deng, Y. Du, S. Cheng, Combustion characteristics of magnesium borides and their agglomerated particles, Combust. Flame 203 (2019) 230-237.

[25]. D. Xu, Y. Jiang, S. Zhang, J. Li, C. Zhao, L. Yang, Screening the thermal oxidation and combustion characteristics of boride particles: a comparative study, Combust. Flame 280 (2025) 114387.

[26]. E.A. Levashov, A.S. Mukasyan, A.S. Rogachev, D.V. Shtansky, Self-propagating high-temperature synthesis of advanced materials and coatings, Inter. Mater. Rev. 62 (2017) 203-239.

[27]. K. Morsi, The diversity of combustion synthesis processing: a review, J. Mater. Sci. 47 (2012) 68-92.

[28]. A. Shiryaev, Thermodynamics of SHS processes: An advanced approach, Int. J. Self-Propagating High-Temp. Synth. 4 (1995) 351-362.

[29]. D.Yu. Kovalev, A.Yu. Potanin, E.A. Levashov, N.F. Shkodich, Phase formation dynamics upon thermal

explosion synthesis of magnesium diboride, Ceram. Int. 42 (2016) 2951-2959.
[30]. V. Rosenband, A. Gany, Thermal explosion synthesis of a magnesium diboride powder, Combust. Explos. Shock Waves 50 (2014) 653-657.
[31]. K. Przybylski, L. Stobierski, J. Chmist, A. Kołodziejczyk, Synthesis and properties of MgB2 obtained by SHS method, Phys. C: Supercond. Appl. 387 (2003) 148-152.
[32]. A.Yu. Potanin, E.A. Levashov, D.Yu. Kovalev, Dynamics of phase formation during the synthesis of magnesium diboride from elements in thermal explosion mode, Russ. J. Non-ferr. Met. 58 (2017) 396-404.
[33]. Y. Takano, N. Oguro, Y. Kaieda, K. Togano, Superconducting properties of combustion synthesized MgB_2, Phys. C: Supercond. Appl. 412-414 (2004) 125-129.
[34]. K. Estala-Rodriguez, S. Cordova, E. Shafirovich, Oxidation and combustion of stabilized lithium metal powder (SLMP), Proc. Combust. Inst. 39 (2023) 3583-3592.
[35]. S. Cordova, K. Estala-Rodriguez, E. Shafirovich, Infiltration-controlled combustion of magnesium for power generation in space, Combust. Flame 238 (2022) 111950.
[36]. M. Miryala, S.S. Arvapalli, P. Diko, M. Jirsa, M. Murakami, Flux pinning and superconducting properties of bulk MgB_2 with MgB_4 addition, Adv. Eng. Mater. 22 (2020) 1900750.
[37]. Z. Zhang, J. MacManus-Driscoll, H. Suo, Q. Wang, Review of synthesis of high volumetric density, low gravimetric density MgB_2 bulk for potential magnetic field applications, Superconductivity 3 (2022) 100015.
[38]. H. Gunda, K.G. Ray, L.E. Klebanoff, C. Dun, M.A.T. Marple, S. Li, P. Sharma, R.W. Friddle, J.D. Sugar, J.L. Snider, R.D. Horton, B.C. Davis, J.M. Chames, Y. Liu, J. Guo, H.E. Mason, J.J. Urban, B.C. Wood, M.D. Allendorf, K. Jasuja, V. Stavila, Hydrogen storage in partially exfoliated magnesium diboride multilayers, Small 19 (2023) 2205487.
[39]. S.K. Padhi, X. Liu, M.C. Valsania, L. Andreo, A. Agostino, A. Alessio, L. Pastero, A. Giordana, Z. Wu, G. Cravotto, M. Truccato, Structure and physicochemical properties of MgB_2 nanosheets obtained via sonochemical liquid phase exfoliation, Nano-Struct. Nano-Objects 35 (2023) 101016.
[40]. S.K. Das, A. Bedar, A. Kannan, K. Jasuja, Aqueous dispersions of few-layer-thick chemically modified magnesium diboride nanosheets by ultrasonication assisted exfoliation, Sci. Rep. 5 (2015) 10522.
[41]. Y. Jiang, D. Ka, A.H. Huynh, J. Baek, R. Ning, S.-J. Yu, X. Zheng, Exfoliated magnesium diboride (MgB_2) nanosheets as solid fuels, Nano Lett. 23 (2023) 7968–7974.
[42]. K.L. Chintersingh, M. Schoenitz, E.L. Dreizin, Boron doped with iron: Preparation and combustion in air, Combust. Flame 200 (2019) 286-295.
[43]. J. Wang, K. Zhong, X. Zeng, Y. Mao, J. Chen, F. Nie, H. Gou, J. Wang, Interfacial oxidation of boron proceeds through a stable B_6O intermediate, Nat. Commun. 16 (2025) 9800.
[44]. M.J. Camarena, Optimization and purification of magnesium borides fabricated by combustion synthesis and by high-temperature sintering, M.S. Thesis, The University of Texas at El Paso, Open Access Theses & Dissertations (2024) 4228.
[45]. V.E. Zarko, The prospects of using nanoenergetic materials in solid rocket propulsion, in: Q.-L. Yan, G.-Q. He, P.-J. Liu, M. Gozin (Eds.), Nanomaterials in Rocket Propulsion Systems, Elsevier, Amsterdam, 2019, pp. 3-30.
[46]. M. Momtaz, J.L. McNanna, M. Schoenitz, E.L. Dreizin, Effect of powder characteristics on thermal oxidation of boron, Thermochim. Acta 743 (2025) 179917.
[47]. P. Biswas, C.H. Pham, M.R. Zachariah, Magnesium-induced strain and immobilized radical generation on the boron oxide surface enhances the oxidation rate of boron particles: A DFTB-MD study, Langmuir 39 (2023) 13782–13789.
[48]. D. Liang, R. Xiao, J. Liu, Y. Wang, Ignition and heterogeneous combustion of aluminum boride and boron-aluminum blend, Aerosp. Sci. Technol. 84 (2019) 1081-1091.
[49]. D. Liang, J. Liu, Y. Zhou, J. Zhou, K. Cen, Ignition and combustion characteristics of molded amorphous boron under different oxygen pressures, Acta Astronaut. 138 (2017) 118-128.
[50]. J. Jovović, S. Stojadinović, N.M. Šišović, N. Konjević, Spectroscopic study of plasma during electrolytic oxidation of magnesium- and aluminium-alloy, J. Quant. Spectrosc. Radiat. Transf. 113 (2012) 1928-1937.
[51]. V. Kaufman, W.C. Martin, Wavelengths and energy level classifications of magnesium spectra for all stages of ionization (Mg I through Mg XII), J. Phys. Chem. Ref. Data 20 (1991) 83-152.
[52]. A. Kramida, Y. Ralchenko, J. Reader, NIST ASD Team, NIST Atomic Spectra Database, National Institute of Standards and Technology, Gaithersburg, MD, 2024. https://physics.nist.gov/asd (accessed September 16, 2025).
[53]. G. Jian, S. Chowdhury, K. Sullivan, M.R. Zachariah, Nanothermite reactions: Is gas phase oxygen generation from the oxygen carrier an essential prerequisite to ignition?, Combust. Flame 160 (2013) 432–437.
[54]. Y. Sato, T. Saito, K. Tsuchiya, M. Terauchi, H. Saito, M. Takeda, Electron energy-loss and soft X-ray emission spectroscopy of electronic structure of MgB_4, J. Solid State Chem. 253 (2017) 58-62.
[55]. S. Hachmioune, A.M. Ganose, M.B. Sullivan, D.O. Scanlon, Exploring the thermoelectric potential of MgB_4: electronic band structure, transport properties, and defect chemistry, Chem. Mater. 36 (2024) 6062-6073.